Adjustment and Extension of the Hansen and Rattray Estuarine Classification Diagram

Dijkstra, Y.M.; Schuttelaars, H.M.

DOI
10.1175/JPO-D-21-0021.1

Publication date
2021

Document Version
Final published version

Published in
Journal of Physical Oceanography

Citation (APA)
Dijkstra, Y. M., & Schuttelaars, H. M. (2021). Adjustment and Extension of the Hansen and Rattray Estuarine Classification Diagram. *Journal of Physical Oceanography*, *51*(9), 2903–2913. https://doi.org/10.1175/JPO-D-21-0021.1

Adjustment and Extension of the Hansen and Rattray Estuarine Classification Diagram

YOERI M. DIJKSTRA[a] AND HENK M. SCHUTTELAARS[a]

[a] *Delft Institute of Applied Mathematics, Delft University of Technology, Delft, Netherlands*

(Manuscript received 28 January 2021, in final form 10 May 2021)

ABSTRACT: The classification diagram developed by Hansen and Rattray is one of the classic papers on classification of estuarine salinity dynamics. However, we found several inconsistencies in both their stratification–circulation and estuarine classification diagrams. These findings considerably change the interpretation of their work. Furthermore, while their classification includes salt wedge estuaries, the model used to derive this is only applicable to well-mixed and partially mixed estuaries. Here, we identify and solve these inconsistencies, and we propose new adjusted and extended stratification–circulation and classification diagrams. To this end, we summarize the model of Hansen and Rattray and extend their work to find analytical model solutions and an adjusted stratification–circulation diagram. Using this new diagram, it is shown that Hansen and Rattray incorrectly discussed the behavior of dispersion-dominated estuaries and that several parts of the diagram correspond to physically unrealistic model solutions. This is then used to demonstrate that several estuarine classes identified by Hansen and Rattray correspond to physically unrealistic model solutions and can therefore not be interpreted. A new and extended classification is proposed by using a recently developed model that extends the work of Hansen and Rattray to salt wedge estuaries. This results in an extended estuarine classification including examples of the location of 12 estuaries in this new diagram.

KEYWORDS: Estuaries; Nonlinear dynamics; Salinity; Classification

1. Introduction

Scientific discussions on salt distribution in estuaries often feature a description in terms of the amount of stratification and the salt regime that describes the primary salt transport processes. One of the most frequently cited contributions related to this is the paper by Hansen and Rattray (1966, hereafter HR66). Their paper is prominently cited in multiple introductory textbooks and review papers on estuarine dynamics (e.g., Fischer et al. 1979; Valle-Levinson 2010; Prandle 2011; MacCready and Geyer 2010; Geyer and MacCready 2014). The main result of HR66 is their estuarine classification diagram. While other classification schemes have appeared more recently (e.g., Scott 1993; Guha and Lawrence 2013; Geyer and MacCready 2014; Dijkstra and Schuttelaars 2021), the Hansen and Rattray classification diagram remains at the basis of estuarine theory. However, we identified that, while their model development is correct, there are several inconsistencies in their classification diagram, which quite drastically alter the diagram and its interpretation. Furthermore, the interpretation of the HR66 classification can be extended by employing a recent model by Dijkstra and Schuttelaars (2021) in which some of the model restrictions made in HR66 were removed to describe more types of estuaries. The goal of this work is therefore to carefully review the theory and diagrams of HR66 and provide an new adjusted and extended version of their work.

Before HR66, classification of the estuarine salinity structure was usually based on the degree of observed stratification, ranging from well-mixed to salt wedge (Pritchard 1955). However, using the subtidal width-averaged model of Hansen and Rattray (1965), HR66 were able to elegantly show that estuarine dynamics cannot be described by just observing the amount of salinity stratification, but at least two parameters describing the flow and stratification should be considered. HR66 selected the ratio of the surface to the mean velocity, or *circulation*, and the relative top–bottom salinity difference, or *stratification*. For each combination of these observable parameters, HR66 determined the relative importance of two primary salt import mechanisms in their model: dispersion attributed to tides and vertical shear dispersion due to gravitational circulation. This is visualized in their well-known *stratification–circulation diagram*. They then use this diagram to propose a classification of estuaries and illustrate a number of examples of estuaries in this classification diagram.

Recently, Dijkstra and Schuttelaars (2021) extended the Hansen and Rattray model by relaxing some of the assumptions. Most notably they retained the advective terms in the momentum equations. This resulted in a fully nonlinear subtidal width-averaged model. Using this model, they showed that the results of the Hansen and Rattray (1965) model are only valid in part of the parameter space, mainly for well mixed and partially stratified estuaries. For the description of estuaries with salinity fronts or subtidal salt wedges, the advective terms in the momentum balance play an essential role for salt transport and the Hansen and Rattray model cannot be applied. Therefore, this model is used to reflect upon the HR66 classification diagram and extend it with the description of estuaries with salt fronts and subtidal salt wedge estuaries.

This paper is structured as follows: section 2 provides a brief summary of the models of Dijkstra and Schuttelaars (2021) and HR66. For the latter, we elaborate on the main assumptions and carefully review some of the main analytical results. Next, in section 3 we present an adjusted stratification–circulation diagram consistent with the HR66 model and an extended

Corresponding author: y.m.dijkstra@tudelft.nl

DOI: 10.1175/JPO-D-21-0021.1

diagram using the nonlinear model of Dijkstra and Schuttelaars (2021). These diagrams are then used to construct an adjusted and extended classification scheme in section 4. Finally, the conclusions are summarized in section 5.

2. Model summary

We provide a summary of the subtidal width-averaged model equations, e.g., as used by Dijkstra and Schuttelaars (2021), and then focus on the simplifying assumptions required to arrive at the model of Hansen and Rattray (1965) and summarize their main results. We largely use the original notation of Hansen and Rattray (1965), only deviating slightly to assist the intuitive interpretation.

a. Equations

The model equations consist of the subtidal width-averaged equations for water motion and salinity applying the hydrostatic assumption, Boussinesq assumption, and rigid lid assumption. Furthermore, a constant and depth uniform vertical eddy viscosity and vertical and horizontal eddy diffusivity are used to parameterize the effects of averaging over turbulence and tidal time scales and over the lateral dimension. The model geometry is restricted to straight channels of constant width B and depth D. The coordinate system (see Fig. 1) consists of an along-channel coordinate x, where $x = 0$ at the mouth and $x < 0$ in upstream direction and dimensionless vertical coordinate η, where $\eta = 1$ denotes the bed and $\eta = 0$ denotes the surface (rigid lid). Hence, the vertical axis is pointing downward. The model solves for the flow velocity u and w in along-channel and vertical direction and salinity s.

The full model consists of the width-averaged continuity equation and conservation of momentum and salinity. The corresponding equations read as

$$u_x + \frac{1}{D} w_\eta = 0, \tag{1}$$

$$-\frac{A_v}{D^2} u_{\eta\eta} + u u_x + \frac{1}{D} w u_\eta = -g\zeta_x + g\beta D \int_\eta^0 s_x \, d\eta', \tag{2}$$

$$-\frac{K_v}{D^2} s_{\eta\eta} + u s_x + \frac{1}{D} w s_\eta = (K_h s_x)_x. \tag{3}$$

Here, g is the acceleration of gravity, K_h is a horizontal dispersion coefficient, and A_v and K_v are the vertical eddy viscosity and eddy diffusivity and are assumed to have the same value (i.e., $A_v = K_v$). The variable β denotes the haline contraction coefficient assuming the density depends linearly on salinity. The variable ζ_x denotes the water-level gradient, which acts here purely as a pressure gradient as the water-level itself is not considered. Subscripts x and η denote derivatives with respect to these variables.

For the bottom and surface boundary conditions, it is assumed that the water motion satisfies no slip and no stress boundary conditions at the bed and surface as well as nonpermeability conditions. The salinity is assumed to satisfy no-flux conditions at both the bed and surface. These conditions are mathematically expressed as

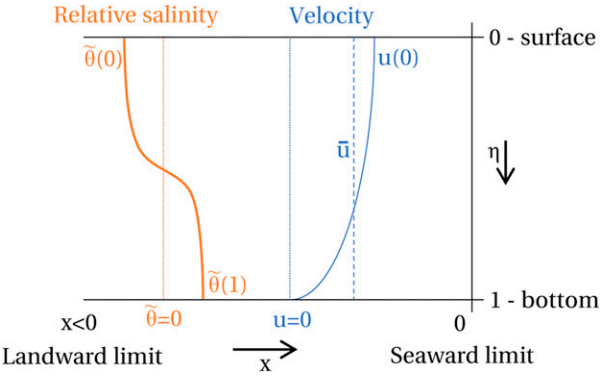

FIG. 1. Sketch of the coordinate system and definition of some symbols related to velocity and the relative salinity [introduced in Eq. (8)].

$$u = 0, \quad \text{at} \quad \eta = 1 \,(\text{bed}), \tag{4a}$$

$$\frac{A_v}{D} u_\eta = 0, \quad \text{at} \quad \eta = 0 \,(\text{surface}), \tag{4b}$$

$$w = 0, \quad \text{at} \quad \eta = 1 \,(\text{bed}), \tag{4c}$$

$$w = 0, \quad \text{at} \quad \eta = 0 \,(\text{surface}), \tag{4d}$$

$$\frac{K_v}{D} s_\eta = 0, \quad \text{at} \quad \eta = 1 \,(\text{bed}), \tag{4e}$$

$$\frac{K_v}{D} s_\eta = 0, \quad \text{at} \quad \eta = 0 \,(\text{surface}). \tag{4f}$$

Note that Dijkstra and Schuttelaars (2021) use a partial slip roughness condition instead of Eq. (4a). For consistency with HR66, we adapted this to a no slip condition for this study.

Horizontal boundary conditions require that salinity vanishes as x tends to $-\infty$ and the flow approaches a barotropic flow profile with net discharge equal to a freshwater discharge R. At the seaward boundary $x = 0$, it is assumed the bottom salinity is fixed to some constant salinity s_{sea} and the salinity profile satisfies Eq. (3) without horizontal diffusion. Mathematically this is expressed as

$$BD \int_1^0 u \, d\eta = R \quad \text{as} \quad x \to -\infty, \tag{5a}$$

$$-g\zeta_x + \frac{A_v}{D^2} u_{\eta\eta} = 0 \quad \text{as} \quad x \to -\infty, \tag{5b}$$

$$u s_x + \frac{w}{D} s_\eta = \frac{K_v}{D^2} s_{\eta\eta} \quad \text{at} \quad x = 0, \ \eta \in [0, 1) \tag{5c}$$

$$s = s_{\text{sea}} \quad \text{at} \quad x = 0, \ \eta = 1, \tag{5d}$$

$$s = 0 \quad \text{as} \quad x \to -\infty. \tag{5e}$$

b. Simplified equations used by Hansen and Rattray

Hansen and Rattray (1965) greatly simplify the above equations by only seeking certain types of solutions. Their solutions assume a uniform horizontal flow velocity in the x direction, linearly decaying salinity in the x direction, and stratification independent of the x coordinate. These assumptions essentially

make the model a water column (1D vertical) model. We will immediately impose these assumptions, which read as

$$u(x,\eta) = u(\eta), \tag{6}$$

$$w(x,\eta) = 0, \tag{7}$$

$$s(x,\eta) = s_0\left[\nu\frac{R}{BDK_{h,0}}x + 1 + \tilde{\theta}(\eta)\right], \tag{8}$$

where ν is a dimensionless parameter indicating the steepness of the along-channel salinity profile and $K_{h,0}$ denotes the horizontal eddy diffusivity at $x = 0$, s_0 is the depth-average salinity at $x = 0$, and $\tilde{\theta}$ is an x-independent vertical salinity profile that still needs to be computed from the model. Note that we deviate slightly from the notation of Hansen and Rattray (1965) by using $\tilde{\theta}$, which equals $\theta - 1$ in their notation and is such that $\tilde{\theta}$ has a depth mean of zero. The horizontal salinity gradient [Eq. (8)] scales with a length scale $BDK_{h,0}/(\nu R)$, which for $\nu \approx 1$ is a typical length scale for diffusive salt transport.

Within this assumed structure, the salinity becomes negative if x becomes a large negative number. To prevent this, Hansen and Rattray consider the model to be valid only in the "inner zone" of the estuary, i.e., with x such that the salinity remains well above zero. In fact, it may be assumed that the model describes a single water column in the estuary and, without loss of generality, we may always simply choose $x = 0$. Additionally, the model is only valid if $\tilde{\theta} > -1$ to prevent negative salinity.

The above assumed form of the solutions is only consistent with the salinity equation [Eq. (3)] for very specific choices of the parameters: it is required to assume longitudinally uniform values for all parameters except for the horizontal eddy diffusivity K_h, which needs to satisfy

$$K_h(x) = K_{h,0} + \frac{R}{BD}x. \tag{9}$$

We can now start to simplify the model using the above assumptions. The continuity equation becomes trivial so that the model consists of simplified momentum and salinity equations. Substituting the expression for u, s, and K_h. from Eqs. (6), (8), and (9) into the model yields:

$$-\frac{A_v}{D^2}u_{\eta\eta} = -g\zeta_x - g\beta s_0\nu\frac{R}{BK_{h,0}}\eta, \tag{10}$$

$$-\frac{K_v}{D^2}\tilde{\theta}_{\eta\eta} = -u\nu\frac{R}{BDK_{h,0}} + \frac{\nu}{K_{h,0}}\left(\frac{R}{BD}\right)^2. \tag{11}$$

The vertical boundary conditions may be rewritten to

$$u = 0, \quad \text{at} \quad \eta = 1\,(\text{bed}), \tag{12a}$$

$$u_\eta = 0, \quad \text{at} \quad \eta = 0\,(\text{surface}), \tag{12b}$$

$$\tilde{\theta}_\eta = 0, \quad \text{at} \quad \eta = 1\,(\text{bed}), \tag{12c}$$

$$\int_1^0 \tilde{\theta} = 0. \tag{12d}$$

TABLE 1. Dimensionless parameters in the Hansen and Rattray (1965) model.

Parameter	Expression	Meaning
Ra	$g\beta s_0 D^3/(A_v K_{h,0})$	Estuarine Rayleigh number
M	$K_v K_{h,0} B^2/R^2$	Tidal mixing-river flow ratio
ν		Salt intrusion length parameter

Note that we no longer need the boundary conditions for w. Furthermore, we may no longer impose the boundary condition for salinity at the surface [Eq. (4f)], as the simplified salinity equation Eq. (11) only allows one Neumann boundary condition. By the choice of the structure of K_h [Eq. (9)] this surface boundary condition for salinity is automatically satisfied in Eq. (3) [this may be verified by inserting Eqs. (6)–(9) in Eq. (3) and integrating once]. Instead, we impose the condition that the depth average of $\tilde{\theta} = 0$.

The imposed structure of the velocity and salinity [Eqs. (6)–(8)] does not satisfy the horizontal boundary conditions. Hence, we use the abovementioned assumption that the model is only valid in the inner zone of the estuary and do not worry about other processes and structures outside of the inner zone that are required to satisfy the boundary conditions. To close the equations, we instead impose conditions that guarantee conservation of mass between the inner zone and the rest of the estuary. Hence, we require that the cross-sectionally integrated transport of water equals the river discharge and the cross-sectionally integrated transport of salt vanishes in equilibrium, i.e.,

$$BD\int_0^1 u\,d\eta = R, \tag{13a}$$

$$BD\int_0^1 (us - K_h s_x)\,d\eta = 0. \tag{13b}$$

c. *Hansen and Rattray solutions*

While Hansen and Rattray (1965) solve for the flow velocity in terms of a streamfunction, we will follow the notationally more convenient method of MacCready (2004) to solve for this model directly in terms of the flow velocity u. Integrating the momentum Eq. (10) and using the boundary conditions (12a) and (12b) and closure condition (13a), we find the velocity

$$\frac{u}{\overline{u}} = \frac{3}{2}(1-\eta^2) + \frac{\text{Ra}}{48}\nu(8\eta^3 - 9\eta^2 + 1), \tag{14}$$

where $\overline{u}$ is the depth-averaged velocity [$=R/(BD)$] and Ra is defined by Hansen and Rattray (1965) as an *estuarine equivalent to the Rayleigh number*, with its definition given in Table 1.

Substituting the solution for the flow velocity in the salinity Eq. (11), integrating, and using boundary conditions (12c) and (12d), we obtain the solution to the depth profile of the salinity

$$\tilde{\theta} = -\frac{15\eta^4 - 30\eta^2 + 7}{120}\frac{\nu}{M} + \nu\frac{\text{Ra}}{48}\frac{48\eta^5 - 90\eta^4 + 60\eta^2 - 10}{120}\frac{\nu}{M}. \tag{15}$$

In this expression, M denotes a dimensionless number representing the ratio of tidal mixing to river flow and is defined in Table 1.

Next, substituting the expressions for velocity and salinity into the closure equation for the salinity transport (13b), results in

$$\underbrace{1}_{\text{river flushing}} \underbrace{-\nu}_{\text{dispersive transport}} = \underbrace{\frac{\nu}{1680M}\left[32+76\frac{\mathrm{Ra}}{48}\nu+\frac{152}{3}\left(\frac{\mathrm{Ra}}{48}\nu\right)^2\right]}_{\text{advective transport}}, \tag{16}$$

where the terms on the left-hand side indicate the salt transport related to flushing by the river and horizontal dispersion. The right-hand side indicates the advective salt transport by vertical shear dispersion.

The closure equation may be regarded as a relation that links the three parameters Ra, M, and ν such that only two out of these parameters may be chosen freely; the value of the third parameter follows from Eq. (16). As we will show in the results below, certain seemingly realistic choices of two parameter values require an unrealistic value of the third parameter. This observation is not discussed in the original work of Hansen and Rattray (1965) or HR66 and is key to our discussion below.

3. Results

a. *Adjusted stratification–circulation diagram using the Hansen and Rattray model*

The classification diagram of HR66 expresses the solutions of the model in terms of three parameters. The first is the *relative circulation* $u(0)/\overline{u}$, i.e., the surface velocity relative to the depth-averaged velocity, which measures the strength of the baroclinic circulation. The second is the *relative stratification* $\Delta\tilde{\theta} = \tilde{\theta}(1) - \tilde{\theta}(0) = [s(x, 1) - s(x, 0)]/s_0$, i.e., the top–bottom salinity difference relative to the depth-average salinity. Note that $\Delta\tilde{\theta}$ can become larger than unity, signifying relatively large stratification with a small average salinity (e.g., a shallow salt wedge in an otherwise freshwater column). The final parameter is ν, a measure for the steepness of the along-channel salinity gradient and relative importance of diffusive processes. New compared to HR66, we found that the stratification $\Delta\tilde{\theta}$ may be explicitly expressed in terms of the circulation $u(0)/\overline{u}$ and ν. This greatly simplifies the construction of the classification diagram. The expression is derived below.

Using the solutions above, the circulation and stratification can be expressed as

$$\frac{u(0)}{\overline{u}} = \frac{3}{2} + \frac{\mathrm{Ra}}{48}\nu, \tag{17}$$

$$\Delta\tilde{\theta} = \frac{15}{120}\frac{\nu}{M} + \frac{18}{120}\nu\frac{\mathrm{Ra}}{48}\frac{\nu}{M}. \tag{18}$$

We first rewrite Eq. (17) to

$$\frac{\mathrm{Ra}}{48}\nu = \frac{u(0)}{\overline{u}} - \frac{3}{2}. \tag{19}$$

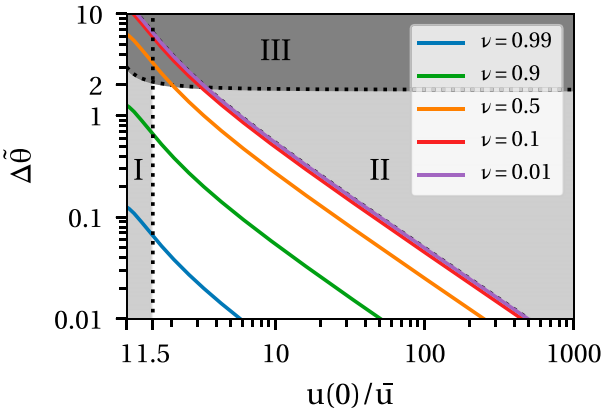

FIG. 2. Stratification–circulation diagram corresponding to the model of Hansen and Rattray (1965) and HR66. The colored lines indicate solutions for several values of ν, obtained using Eq. (21). The gray-shaded regions indicate unpermitted or unlikely solutions (see the text for an extensive discussion).

Substituting this expression for $(\mathrm{Ra}/48)\nu$ in Eq. (16) and rewriting we find

$$M = \frac{38\nu\left[\frac{u(0)}{\overline{u}}\right]^2 - 57\nu\left[\frac{u(0)}{\overline{u}}\right] + 24\nu}{1260(1-\nu)}. \tag{20}$$

Finally, substituting the expressions for $(\mathrm{Ra}/48)\nu$ and M in Eq. (18) we find

$$\Delta\tilde{\theta} = 63(1-\nu)\frac{3\left[\frac{u(0)}{\overline{u}}\right] - 2}{38\left[\frac{u(0)}{\overline{u}}\right]^2 - 57\left[\frac{u(0)}{\overline{u}}\right] + 24}. \tag{21}$$

This new expression makes it very easy to construct the stratification–circulation diagram for any value of ν. Figure 2 shows the curves described by Eq. (21) for several values of ν indicated by the various colored lines. The lines are almost straight (in log–log scale) and downsloping as $u(0)/\overline{u}$ increases. Note that for $u(0)/\overline{u} > 2/3$ and $0 < \nu < 1$, both the numerator and denominator in Eq. (21) are positive and hence $\Delta\tilde{\theta}$ is positive.

The above expressions allow us to provide an in-depth interpretation of the stratification–circulation diagram of Fig. 2. To this end, we first consider the case $0 < \nu < 1$ within the white region of the figure. Next, we will consider the validity of the results within three gray-shaded regions in the figure indicated by I, II, and III, which will also feature the cases $\nu > 1$ and $\nu < 0$.

1) CASE $0 < \nu < 1$ (WHITE REGION)

Hansen and Rattray (1965) show that ν may be interpreted as the relative importance of dispersive salt transport over advective salt transport due to shear dispersion. Hence, as $0.5 < \nu < 1$, the salt transport is dominated by a balance between horizontal dispersion and river flushing. From Fig. 2 it follows that this corresponds to either a relatively

small stratification or circulation. For ν increasing toward 1, stratification gradually vanishes. Conversely, for values of $0 < \nu < 0.5$, the salt transport becomes dominated by the balance between river flushing and advective transport. From Fig. 2 it follows that such advection-dominated estuaries can be found for either relatively large stratification and small circulation or small stratification and large circulation.

Special attention should be paid to the case of ν closely approaching either 0 or 1. For ν approaching zero, by Eq. (20) M has to approach zero as well (i.e., no mixing relative to the freshwater input). Similarly, for ν approaching 1, M has to approach infinity (i.e., infinite mixing or no freshwater input). This can only happen for very extreme choices of the mixing parameters or river discharge and therefore should be considered as limiting cases. It can be shown that the most extreme limiting cases of $\nu = 0$ or $\nu = 1$ no longer describe an estuary. We refer to appendix A for a detailed description of these extremes.

Assuming $0 < \nu < 1$, the circulation always remains larger than 3/2. The limit value $u(0)/\overline{u} = 3/2$ corresponds to a circulation resulting from only a barotropic river discharge without any gravitational circulation. According to Eq. (17) this can only happen when Ra tends to zero, representing infinite mixing. Any value of $u(0)/\overline{u}$ larger than 3/2 means some gravitational circulation is present.

2) Regions I, II, and III

Figure 2 furthermore shows three gray shaded regions, which describe not permitted or unlikely solutions. Region I is located left of the line $u(0)/\overline{u} = 3/2$ and denotes solutions with a circulation smaller than 3/2 and larger than 2/3. Within this model, this can only occur if gravitational circulation is oppositely directed (i.e., inflow at the surface, outflow at the bottom). To analyze this, we distinguish three cases. First, for $0 < \nu < 1$ it follows that $\mathrm{Ra} < 0$, $M > 0$ [Eqs. (19) and (20)]. Looking at the definitions of Ra and M (Table 1) there is no physically realistic choice of parameters to achieve this. Second, for $\nu < 0$, $\mathrm{Ra} > 0$ and $M < 0$, which can again not be attained in any physically realistic way. Finally, for $\nu > 1$ it follows that $\mathrm{Ra} < 0$, $M < 0$, which can only somewhat realistically be obtained by requiring $K_{h,0} < 0$ and thus an inversion of the salinity gradient [see Eq. (8)]. At the same time, salinity stratification becomes unstable [Eq. (18)]. While this may occur in rare cases in the field, this requires at least some forcing that is not included in this model. Thus, region I cannot be attained by any physically realistic parameter setting within the model assumptions.

Region II is located right of the asymptote for $\nu \to 0$ and corresponds to values of $\nu < 0$ by Eq. (21). As in region I, this means that $\mathrm{Ra} < 0$, $M < 0$ [Eqs. (19) and (20)], which can only be somewhat realistically established by choosing $K_{h,0} < 0$. By choosing both ν and $K_{h,0}$ negative, the salinity gradient remains positive [i.e., decreasing salinity in up-estuary direction, Eq. (8)] and these estuaries are stably stratified. These estuaries are thus special in the sense that the dispersion term is causing export of salt, which may be possible theoretically. We argue that this is only reserved for rare cases and should be considered unlikely (for a further discussion, see section 4).

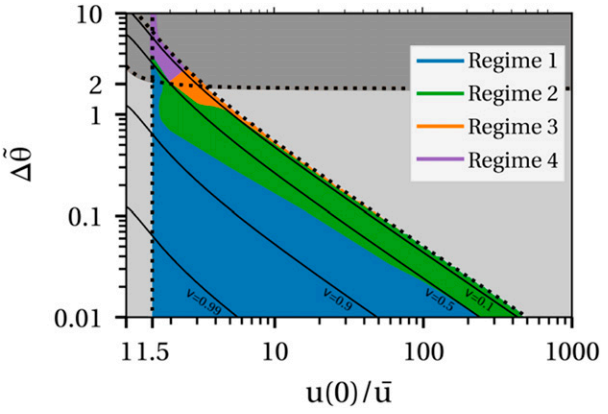

FIG. 3. Stratification–circulation diagram corresponding to the nonlinear model as measured midestuary. The colors indicate the regimes as defined by Dijkstra and Schuttelaars (2021). Solutions for several values of ν from the HR66 model are plotted for reference.

Finally, region III is located at the top of the figure and indicates the region where $\tilde{\theta}(0) < -1$, which, using realistic (i.e., positive) values for all model parameters would result in negative salinities. This is obviously not permitted. Mathematically such negative salinities occur for $\Delta\tilde{\theta} > \{9[u(0)/\overline{u}] - 6\}/\{5[u(0)/\overline{u}] - 4\}$. The derivation of this relation is presented in appendix B.

b. *Extended stratification–circulation diagram using the fully nonlinear model*

The stratification–circulation diagram can also be constructed using the fully nonlinear model. The model is applied to a straight rectangular channel with along-channel uniform parameters. In contrast to the HR66 model, the fully nonlinear model resolves the entire along-channel range of the estuary and is thus a full 2D model as given by Eqs. (1) and (2) and boundary conditions (4a)–(5e). As the model needs to be solved numerically, the diagram is constructed by running a large number of model simulations for different model parameters. The results are visualised in the diagram of Fig. 3. On the axes, we have used the stratification and circulation occurring midestuary, i.e., at $x = (1/2)L_s$, where L_s is the salt intrusion length measured as the distance from $x = 0$ to the 1-psu line.

The diagram indicates four regions corresponding to the four regimes identified by Dijkstra and Schuttelaars (2021). The *regime* in this context is used to refer to the balance of essential salt transport processes. The four regimes are 1) the dispersive regime (blue) dominated by import due to horizontal dispersion and export due to river flushing; 2) the Chatwin regime (green) dominated by import due to shear dispersion related to gravitational circulation and export due to river flushing; 3) Chatwin regime with advection-dominated front (orange), which is similar to the Chatwin regime but with import at the salt intrusion limit dominated by momentum advection, leading to the formation of a front-like salinity profile; and 4) the subtidal salt wedge regime (magenta) dominated by shear dispersion processes related to momentum

advection for both import and export. Additionally, four solutions for different values of ν from the HR66 model are plotted.

The dominant importing mechanisms in regimes 1 and 2, horizontal dispersion and gravitation circulation are also described by HR66. In the HR66 model, the effect of horizontal dispersion on the salt intrusion dominates for $\nu > 0.5$, while the effect of gravitational circulation dominates for $\nu < 0.5$ In our results, the transition between regimes 1 and 2 occurs for $\nu = 0.5$ for large circulation but may occur for much higher values of ν at smaller values of the circulation. The transition between the regimes is not on the $\nu = 0.5$ line, as the nonlinear model determines the regime based on the dominant mechanism in the entire estuary, not only the dominant mechanism at one point as is done in HR66.

Regimes 3 and 4 highlight the importance of momentum advection, which was neglected by Hansen and Rattray. Regime 3 is found in the area with small ν, including a thin region with ν close to zero for large values of the circulation and admitting larger ν for more moderate values of the circulation. There is no clear line of constant ν that marks the transition between regimes 2 and 3. Regime 4 is found for small values of the circulation and is entirely located in the invalid region III in the HR66 diagram, where stratification is large. Negative salinities occur in Hansen and Rattray's model but not in the nonlinear model. While regimes 3 and 4 seem to occur only in a very small part of the parameter space, this does not mean that these regimes are insignificant: please note that the view is somewhat distorted by the double logarithmic scale.

Results of the nonlinear model mostly respect the boundaries of the feasible region derived for the Hansen and Rattray model. No solutions are found in invalid region I, as the along-channel salinity gradient does not invert and hence the circulation remains larger than 1.5. Also hardly any solutions are found in invalid region II using the nonlinear model. This is because the relative importance of dispersive transport to river flushing is still well approximated by ν in the nonlinear model. Hence, for $\nu \to 0$ dispersion should vanish, meaning $s_x \to 0$ and the salt intrusion length tends to infinity. This is a limiting case, and no solutions exist right of the line $\nu = 0$. An exception to this occurs in regime 4 for circulation close to 1.5, where the dispersive transport no longer primarily scales with the depth-averaged salinity but with the local salinity (i.e., varying in vertical direction). As a consequence, ν is no longer a good measure for the relative effect of dispersion over river flushing and the line $\nu = 0$ loses relevance.

4. Discussion

The presented results first show that the stratification–circulation diagram of Fig. 2 has some important differences with the original stratification–circulation diagram of HR66, which we will discuss below in section 4a. Next, we will show that the original classification scheme of HR66 needs to be reinterpreted using our results in section 4b. Finally, we present an adjusted and extended version of the HR66 classification diagram in section 4c.

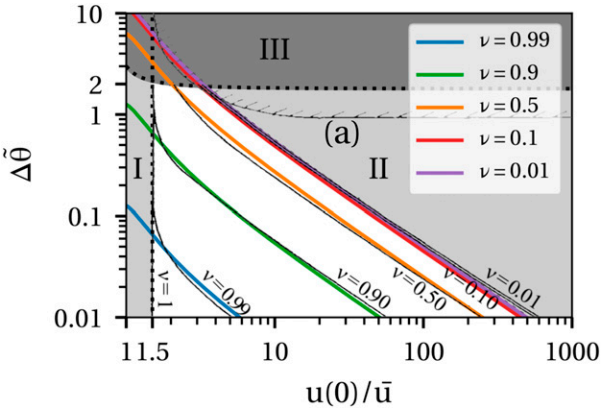

FIG. 4. Stratification–circulation diagram from Fig. 2 compared to the original version published in HR66. The line denoted by "(a)", representing cases with $s = 0$ at the surface, originally appears in the HR66 classification diagram and has been added into this figure.

a. *Comparison to the original stratification–circulation diagram of Hansen and Rattray*

Figure 2 of the stratification–circulation diagram is plotted again in Fig. 4 but now together with the original figure by HR66. We observe several differences. First, we focus on the lines for $\nu = 0.01$, 0.1, 0.5, 0.9, and 0.99. These correspond fairly closely in both figures for $u(0)/\bar{u} > 2$. The small differences may possibly be attributed to less accurate computing and drawing by HR66. The solutions however become completely different for $u(0)/\bar{u}$ decreasing toward 3/2. The solutions drawn by Hansen and Rattray have an asymptote at $u(0)/\bar{u} = 3/2$, moving toward infinite stratification. This is incorrect, as our solution shows the lines simply continue into the area $u(0)/\bar{u} < 3/2$, where the solution can only be obtained using unrealistic parameter values (see results for region I above).

Second, the line $\nu = 1$ in the original diagram is found at $u(0)/\bar{u} < 3/2$ and with any value of the stratification. This is incorrect, as we showed that stratification vanishes as ν approaches 1 and is zero for $\nu = 1$ at which point the salinity becomes constant in the entire estuary. This changes the interpretation of the figure: whereas the original figure suggests that estuaries with ν close to 1 may have any amount of stratification, our correction shows that such estuaries should be characterized by a limited amount of stratification within the Hansen and Rattray model.

Finally, we focus on the line marked by "(a)" at the top of the figure. This line originally only features in the classification diagram of HR66 but we copied it to the stratification–circulation diagram as it is more appropriate to discuss here. The original paper does not explain how this line is derived, simply that it represents "conditions of freshwater outflow over a stagnant saline layer." This implies that it should correspond to a solution of $s = 0$ at the surface. Hence, line (a) should correspond to our boundary of region III. These two lines clearly do not correspond. As a consequence Hansen and Rattray incorrectly allow for a part of the parameter space of

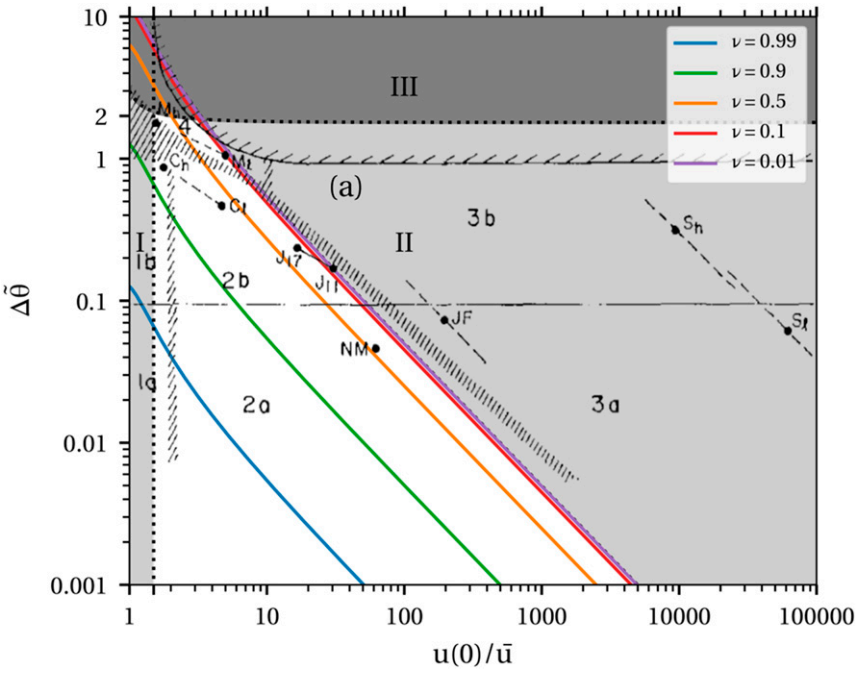

FIG. 5. Classification diagram of HR66 overlaid with the adjusted stratification–circulation diagram. This figure shows that part of the classified area by HR66 is actually within the gray-shaded regions that correspond to unpermitted or physically unrealistic solutions.

highly stratified estuaries ($\Delta\tilde{\theta} > 2$) with small circulation [$3/2 < u(0)/\overline{u} < 3$], while such estuaries may actually not exist according to their model.

b. Consequences for the estuarine classification diagram

HR66 use their stratification–circulation diagram to indicate seven different estuary types. Here we specifically use the word *type*, not regime, as the estuary types of HR66 do not distinguish the essential balance of transport processes but are based on other characteristics. In this section we reflect on the validity of the estuary types of HR66. Figure 5 shows their classification diagram with estuary types denoted with 1a, 1b, 2a, 2b, 3a, 3b, and 4, together with our corrected solution of the stratification–classification diagram. The figure also includes several examples of estuaries as given by HR66 indicated by dots with solid or dashed lines to indicate the natural variation of parameters in these estuaries. We will discuss the estuary types identified by HR66 and evaluate their interpretation using the corrected diagram and the results of the nonlinear model.

Type 1 describes estuaries with unidirectional flow directed seaward in the entire water column, which occurs for $u(0)/\overline{u} < 2$. Using our results, we add the requirement that $u(0)/\overline{u} < 3/2$ to get any results that are meaningful within the context of the model. Type 2 describes estuaries with a bidirectional flow and some nonnegligible role of dispersion in the salt transport (i.e., $\nu = 0.01$). This definition is consistent within the context of the model. The labels a and b in the classification indicate small and large stratification, respectively. Note that neither of these types distinguish the dominant salt transport mechanism.

Type 3 is defined as estuaries dominated by advective processes, i.e., shear dispersion due to gravitational circulation, and are found right of the line $\nu = 0.01$ in Fig. 5. However, as we have shown, only estuaries with ν between 0.01 and 0 can be described using realistic parameter settings. Hansen and Rattray provide two examples of type 3 estuaries right of the line $\nu = 0$, which we denoted as region II: JF (strait of Juan de Fuca) and S (Silver bay at high and low river discharge, indicated by subscripts h and l). This may be possible if these estuaries are characterized by negative dispersive salt transport, but, more likely, these examples do not satisfy the model assumptions: both examples are deep fjord-like systems where the bottom boundary layer is much smaller than the water depth. Hence, the assumptions that the flow and salinity profiles are dominated by bottom friction is no longer valid and it is essential to account for vertical stratification to obtain any realistic estimate of the circulation. Therefore, these examples should not be interpreted using this model.

Finally, type 4 denotes the salt wedge estuaries and is defined by HR66 as a corner of the parameter space with relatively large stratification. This is done rather arbitrarily, as their model is not able to resolve salt wedge–type estuaries. Indeed, the chosen corner of the parameter space is almost entirely located in region III, in which negative salinity occurs in the HR66 model. Nevertheless, a comparison of this type to the subtidal salt wedge regime in the nonlinear model (cf. Fig. 3) shows that HR66 have placed the salt wedge estuaries in the correct corner of the parameter space.

Looking at the definitions of the estuary types of HR66, it should be noted that these are all based on different

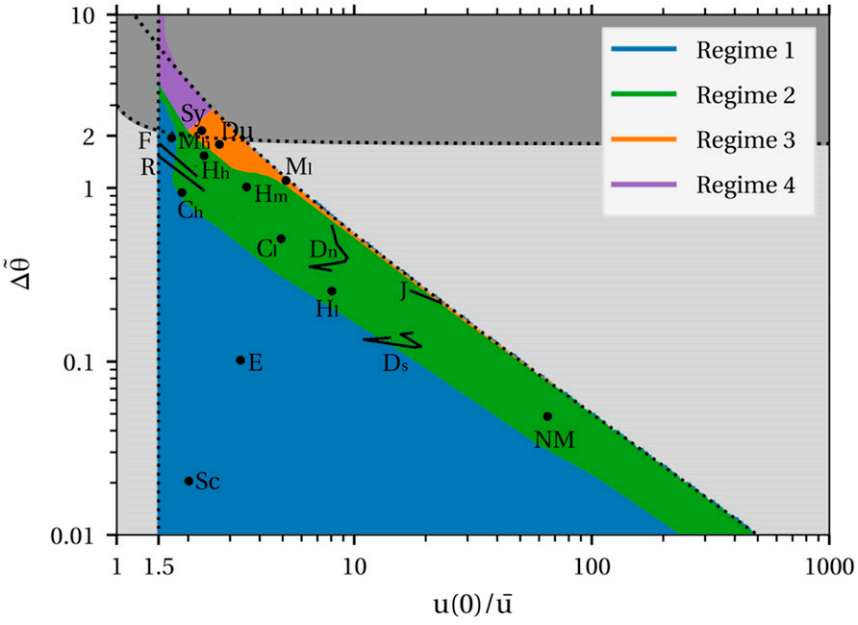

FIG. 6. Adjusted and extended diagnostic classification diagram based on the regimes of Dijkstra and Schuttelaars (2021). Several estuaries are indicated using dots, denoting single locations in an estuary, or lines, denoting an along-channel stretch of the estuary. These examples are derived based on published observations or realistic model results. The letters indicate: C: Columbia (United States), D: Delaware (United States), Du: Duwamish (United States), E: Ems (Germany), F: Fraser (Canada), H: Hudson (United States), J: James (United States) M: Mississippi (United States), NM: Mersey Narrows (United Kingdom), R: Rotterdam Waterway (branch of the Rhine-Meuse delta, Netherlands), Sc: Scheldt (Belgium, Netherlands), Sy: Strymon (Greece). Subscripts *l*, *m*, and *h* denote low, moderate, and high river discharge. Subscripts *s* and *n* denote spring and neap. Note that the locations of these examples are only valid approximately and may vary with flow conditions and use of data at different locations along the length and cross section of the estuary. Additionally, as obtaining subtidal quantities in tidal environments is error-prone, the data or models used to plot these examples may be inaccurate. The reader is referred to appendix C for details on how these examples were derived. Note that there are some minor differences compared to the classification of these estuaries by Dijkstra and Schuttelaars (2021) because they considered the stratification and circulation at $x = 0$ in their model, while this figure considers these quantities midestuary.

characteristics: the shape of the velocity profile (type 1 and 2), the dominant transport mechanism (type 3), and the shape of the salinity profile (type 4). Thus, this classification scheme does not uniformly distinguish between either different salt transport mechanisms (i.e., the regime), flow structure, or salinity structure.

c. *New classification diagram*

We propose to define classification of estuaries uniformly based on either regime, flow structure or salinity structure. In this context we prefer to use regimes and the corresponding classification is given by Fig. 3. This diagram is repeated in Fig. 6 with the location of several estuaries indicated. The examples include estuaries from HR66 that were in the realistic part of the parameter space, as well as eight other estuaries. The location of these estuaries in the parameter space is derived based on published observations or model results at a particular location and under particular conditions. Hence, these locations in the parameter space may vary along the estuary and with varying flow conditions. Additionally, it should be noted that both models and observations may contain significant errors in determining subtidal velocity and salinity in a tidal environment, so the plotted examples may be subject to inaccuracies. More information on the way these locations in the parameter space have been determined is provided in appendix C. Finally, it should be noted that Dijkstra and Schuttelaars (2021) compared the data of these estuaries to the stratification and circulation at $x = 0$ in their model, while here this is compared to the stratification and circulation midestuary. As a result, some of the estuaries appear in a slightly different position in the graph. Specifically, the Rotterdam Waterway and Columbia River at high discharge have (partly) just moved across the boundary from regimes 1 to 2. As the regimes should be regarded as a continuum (see Dijkstra and Schuttelaars 2021), this is actually not such a big difference.

Some of the estuaries plotted, including the Rotterdam Waterway, Fraser, and Hudson at high discharge are strongly stratified or salt wedge–type estuaries with strong variability

over the tidal cycle. Related to the dominant role of the tides, these estuaries are in the dispersion-dominated regime (regime 1) in our classification diagram. This regime also features the tide-dominated well-mixed Ems and Scheldt estuaries. Hence, we want to stress that different types of estuaries may be found in regime 1, as different mechanisms may be associated with the dispersion coefficient in the subtidal width-averaged model. Further research is needed to define a mechanistic classification distinguishing these different types of estuaries in regime 1.

The classification diagram in Fig. 6 is a diagnostic classification (Geyer 2010), i.e., the parameters on its axes may only be determined by closely observing or modeling the local velocity and salinity in the estuary. Its counterpart, the classification diagram presented by Dijkstra and Schuttelaars (2021) depends on the parameter $F_r = R/\sqrt{g\beta s_0 D}$ and Ra (see Table 1) and is prognostic (Geyer 2010), i.e., the parameters may be determined based on more global observations of the estuary and bulk estimates. However, some of the parameters needed for the diagram of Dijkstra and Schuttelaars (2021), especially the horizontal dispersion parameter and eddy viscosity, are hard to determine. Therefore, the diagnostic classification in Fig. 6 is often more practical. The classification diagrams are otherwise equivalent and are complementary as they highlight different interpretations of the same theory.

5. Conclusions

We have revisited the model of Hansen and Rattray (1965) and HR66 and have made several adjustments to correct their stratification–circulation and classification diagrams. Furthermore, we have used a recently developed nonlinear model to extend the stratification–circulation diagrams to estuaries with advection-dominated fronts and subtidal salt wedge estuaries. Specifically, we have identified that estuaries with ν close to 1 (strongly dominated by dispersion) should always have small stratification and that several regions of the parameter space cannot be attained using physically realistic parameter settings. The extension using the nonlinear model turns out to be a natural extension that largely results in salinity-circulation patterns that are in the same regions of physically realistic parameter settings in the stratification–circulation diagram of HR66.

We have also revisited the classification diagram of HR66. It was identified that several estuary types defined by HR66 are actually largely located in parts of the parameter space corresponding to physically unrealistic parameter settings. This means that one cannot interpret these types of estuaries using the HR66 model. Additionally, it was identified that Hansen and Rattray's estuary types do not uniformly distinguish between estuaries with different flow structure, salinity structure or dominant salt transport mechanisms, so that the defined types are somewhat arbitrary. To overcome these issues, we proposed an adjusted and extended classification diagram using the regimes of Dijkstra and Schuttelaars (2021), which uniformly distinguish between estuaries with different dominant salt transport mechanisms. The location of 12 estuaries within this parameter space has been indicated. The resulting diagram is equivalent to the classification diagram of Dijkstra and Schuttelaars (2021) but on different axes and may be used complementary.

Acknowledgments. This research was funded by the Dutch Science Organisation (NWO, Grant ALWSD.2016.015).

APPENDIX A

Case ν Approaching 0 and 1

Specific attention should be given to the meaning of ν approaching 0 and 1. First note that $\nu = 0$ corresponds to a zero velocity gradient and may never satisfy the transport equation Eq. (16) unless $s = 0$ everywhere. Thus $\nu = 0$ does not describe an estuary. For ν approaching zero, M is required to approach zero as well in order to balance Eq. (16), in such a way that ν/M remains finite. This may happen in two ways (see Table 1). First, mixing (K_v and A_v or K_h) may decrease toward zero. This means that not only M decreases toward zero but also Ra increases to infinity in such a way that Raν remains finite. In the stratification–circulation diagram, this corresponds to an asymptote just right of the line drawn for $\nu = 0.01$. Alternatively, the river discharge may increase toward infinity with finite mixing. This means that Ra remains finite and the circulation should tend to 3/2 [Eq. (17)]. Thus, the solution tends to one point on the intersection between the asymptotic solution for $\nu \to 0$ and the line $u(0)/\overline{u} < 3/2$, which is not a valid solution of the model. Concluding, ν can only decrease toward zero for vanishing mixing and can never attain zero.

The case $\nu = 1$ requires $M^{-1} = 0$ [Eq. (16)], which may only be established by $R = 0$. This implies no stratification [$\Delta\tilde{\theta} = 0$, see Eq. (18)] and no along-channel salinity gradient [Eq. (8)], and hence a constant salinity in the entire domain. Also this case does not correspond to an estuary. For ν approaching 1 we should require $M \to \infty$, which implies directly that stratification vanishes [Eq. (18)]. To determine the corresponding circulation we need to consider the way in which M increases. First, this may be established by increasing mixing (K_v and A_v or K_h). This means that Ra decreases toward zero and hence circulation tends to 3/2 [Eq. (17)]. Second, M may be increased by decreasing the river discharge to zero. The circulation can then attain any value but the meaning of the circulation is insignificant as it measures the circulation relative to a very small net flow. Concluding, increasing ν toward 1 always means vanishing stratification with either circulation tending to 3/2 or with flow vanishing altogether.

APPENDIX B

Derivation of Region III

Here we provide the derivation of region III in Fig. 2, the region where $s(0) < 0$. From Eq. (8) we note that $s(0) = 0$ at $x = 0$ if $\tilde{\theta} = -1$. Evaluating Eq. (15) for $\tilde{\theta}$ at $\eta = 0$, we find

$$\tilde{\theta}(0) = -\left(\frac{7}{120} + \frac{10}{120}\nu\frac{\mathrm{Ra}}{48}\right)\frac{\nu}{M} = -1.$$

Combining this with Eq. (19), which gives an expression for $\nu(\mathrm{Ra}/48)$, we find an expression for ν/M, which reads as

$$\frac{\nu}{M} = \left[-\frac{8}{120} + \frac{10}{120}\frac{u(0)}{\overline{u}}\right]^{-1}.$$

Next, substituting this and Eq. (19) in Eq. (18) for the stratification $\Delta\tilde{\theta}$, we obtain

$$\Delta\tilde{\theta} = \frac{9\dfrac{u(0)}{\overline{u}} - 6}{5\dfrac{u(0)}{\overline{u}} - 4}.$$

Region III in the stratification–circulation diagram is the region above this line.

APPENDIX C

Location of Estuaries in the Parameter Space

Figure 6 shows the location of several estuaries in the parameter space. These locations have been derived on the basis of observations and model results. Below is a summary of which data were used and how the stratification and circulation were determined for each plotted estuary. The Columbia, James, Mississippi, and Mersey are not mentioned below: these examples have been copied directly from HR66.

a. Delaware

Stratification and circulation in the Delaware were based on 3D model results presented in Figs. 5c, 5d, 13b, and 14a of Aristizábal and Chant (2013) for the case $Q = 650\,\mathrm{m^3\,s^{-1}}$ and spring/neap tidal conditions. We show results between 30 and 50 km, in the middle part of the estuary. The top–bottom salinity difference along the thalweg is presented in Fig. 13b, while the mean salinity is plotted in Fig. 14a. Additionally they computed values of ν based on their model results (Fig. 5 in their paper). We have used the combination of the stratification and ν to infer the circulation used in the Hansen and Rattray model. Note that salinity data are based on results along the thalweg, while ν is computed based on cross-sectionally integrated salt transport.

b. Duwamish

Data for the Duwamish were derived from Fig. 4 of McKeon et al. (2021) for a river discharge of $65\,\mathrm{m^3\,s^{-1}}$ at a location 7.5 km from the mouth, which shows subtidal velocity profiles and salinity during ebb and flood. The surface velocity was derived from this figure, while the average velocity was determined by dividing the river discharge by the local cross-sectional area. The stratification was estimated as an average of the ebb and flood salinity.

c. Ems

Stratification and circulation in the Ems were based on a combination of observations and model results presented by Talke et al. (2009). They present vertical salinity observations from 2 August 2006 during ebb and flood along the thalweg. As salinities during both parts of the tide were similar at 64 km (average salinity ~10 psu) we took the average as an estimate of the mean salinity and stratification. Velocities were not measured and hence the circulation is based on only the river flow and gravitational circulation as computed in their model. This may not equal the actual circulation as it may be observed but is consistent with the meaning of the circulation in HR66.

d. Fraser

Kostaschuk et al. (1992) presents observations of the average salinity and velocity during ebb and flood along the thalweg on 6 June 1987 during fairly high discharge conditions ($Q = 6000\,\mathrm{m^3\,s^{-1}}$). The average of the ebb and flood conditions were used to estimate subtidal quantities. Observations at 0 (mouth) and 3 km were used.

e. Hudson

Data for the Hudson were taken from Figs. 6 and 8 of Ralston et al. (2008). They present observations of the time-averaged vertical velocity profile (Fig. 8), which were used to determine the surface velocity. The mentioned discharge and cross-sectional area are divided to determine the average velocity. The time-averaged top–bottom salinity reported in Fig. 6 was used, and the depth-averaged salinity was taken as the mean of the top and bottom salinities. Three discharge cases in the year 2004 have been considered: low ($400\,\mathrm{m^3\,s^{-1}}$, day 190), moderate ($1200\,\mathrm{m^3\,s^{-1}}$, day 86), and high ($2200\,\mathrm{m^3\,s^{-1}}$, day 92) measured at Hastings (33 km, mean salinity between 3 and 13 psu).

f. Rotterdam Waterway

Data was used from Fig. 2 of De Nijs et al. (2011), which presents the vertical–temporal structure of the flow velocity and salinity observed on 11 April 2006. Discharges were above average (4400–5800 $\mathrm{m^3\,s^{-1}}$ at Lobith). The data were time-averaged to find the subtidal circulation and stratification. Data from station 1 (~7 km from the mouth) and 2 (~18 km) were used.

g. Scheldt

Top–bottom salinity data for the Scheldt were taken from the permanent measurement station at Boei 84 (~60 km) for the months January–May 2015 (Vanlierde et al. 2016). As stratification is small, the depth-averaged salinity is taken to equal the average of the top and bottom salinities. No reliable subtidal velocities are available and hence the circulation is based only on the river flow and gravitational circulation as computed by Brouwer et al. (2015). This may not equal the actual circulation as it may be observed but is consistent with the meaning of the circulation in HR66.

h. Strymon

Observations by Haralambidou et al. (2010) were used. Their Fig. 2 presents vertical profiles of velocity and salinity measured in the summer of 2003 at 2 km.

REFERENCES

Aristizábal, M. F., and R. J. Chant, 2013: A numerical study of salt fluxes in Delaware Bay Estuary. *J. Phys. Oceanogr.*, **43**, 1572–1588, https://doi.org/10.1175/JPO-D-12-0124.1.

Brouwer, R. L., G. P. Schramkowski, T. Verwaest, and F. Mostaert, 2015: Geïdealiseerde processtudie van systeemovergangen

naar hypertroebelheid. WP 1.3 Basismodel getij en zout (in Dutch). Tech. Rep. WL2015R13_103, Flanders Hydraulics Research, Antwerp, Belgium, 72 pp.

De Nijs, M. A. J., J. D. Pietrzak, and J. C. Winterwerp, 2011: Advection of the salt wedge and evolution of the internal flow structure in the Rotterdam Waterway. *J. Phys. Oceanogr.*, **41**, 3–27, https://doi.org/10.1175/2010JPO4228.1.

Dijkstra, Y. M., and H. M. Schuttelaars, 2021: A unifying approach to subtidal salt intrusion modeling in tidal estuaries. *J. Phys. Oceanogr.*, **51**, 147–167, https://doi.org/10.1175/JPO-D-20-0006.1.

Fischer, H. B., E. J. List, R. C. Y. Koh, and J. Imberger, 1979: *Mixing in Inland and Coastal Waters*. Academic Press, 483 pp.

Geyer, W. R., 2010: Estuarine salinity structure and circulation. *Contemporary Issues in Estuarine Physics*, A. Valle-Levinson, Ed., Cambridge University Press, 12–26.

——, and P. MacCready, 2014: The estuarine circulation. *Annu. Rev. Fluid Mech.*, **46**, 175–197, https://doi.org/10.1146/annurev-fluid-010313-141302.

Guha, A., and G. A. Lawrence, 2013: Estuary classification revisited. *J. Phys. Oceanogr.*, **43**, 1566–1571, https://doi.org/10.1175/JPO-D-12-0129.1.

Hansen, D. V., and M. Rattray, 1965: Gravitational circulation in straits and estuaries. *J. Mar. Res.*, **23**, 104–122.

——, and ——, 1966: New dimensions in estuary classification. *Limnol. Oceanogr.*, **11**, 319–326, https://doi.org/10.4319/lo.1966.11.3.0319.

Haralambidou, K., G. Sylaios, and V. A. Tsihrintzis, 2010: Salt-wedge propagation in a Mediterranean micro-tidal river mouth. *Estuarine Coastal Shelf Sci.*, **90**, 174–184, https://doi.org/10.1016/j.ecss.2010.08.010.

Kostaschuk, R. A., M. A. Church, and J. L. Luternauer, 1992: Sediment transport over salt-wedge intrusions: Fraser River estuary, Canada. *Sedimentology*, **39**, 305–317, https://doi.org/10.1111/j.1365-3091.1992.tb01040.x.

MacCready, P., 2004: Toward a unified theory of tidally-averaged estuarine salinity structure. *Estuaries*, **27**, 561–570, https://doi.org/10.1007/BF02907644.

——, and W. R. Geyer, 2010: Advances in estuarine physics. *Annu. Rev. Mar. Sci.*, **2**, 35–58, https://doi.org/10.1146/annurev-marine-120308-081015.

McKeon, M. A., A. R. Horner-Devine, and S. N. Giddings, 2021: Seasonal changes in structure and dynamics in an urbanized salt wedge estuary. *Estuaries Coasts*, **44**, 589–607, https://doi.org/10.1007/s12237-020-00788-z.

Prandle, D., 2011: *Estuaries. Dynamics, Mixing, Sedimentation and Morphology*. Cambridge University Press, 236 pp.

Pritchard, D. W., 1955: Estuarine circulation patterns. *Proc. Amer. Soc. Civ. Eng.*, **81**, 1–11.

Ralston, D. K., W. R. Geyer, and J. A. Lerczak, 2008: Subtidal salinity and velocity in the Hudson River estuary: Onbservations and modelling. *J. Phys. Oceanogr.*, **38**, 753–770, https://doi.org/10.1175/2007JPO3808.1.

Scott, C. F., 1993: Canonical parameters for estuary classification. *Estuarine Coastal Shelf Sci.*, **36**, 529–540, https://doi.org/10.1006/ecss.1993.1032.

Talke, S. A., H. E. De Swart, and H. M. Schuttelaars, 2009: Feedback between residual circulations and sediment distribution in highly turbid estuaries: An analytical model. *Cont. Shelf Res.*, **29**, 119–135, https://doi.org/10.1016/j.csr.2007.09.002.

Valle-Levinson, A., 2010: Definition and classification of estuaries. *Contemporary Issues in Estuarine Physics*, A. Valle-Levinson, Ed., Cambridge University Press, 1–11.

Vanlierde, E., and Coauthors, 2016: MONEOS—jaarboek monitoring WL 2015. Factual data rapportage van monitoring hydrodynamiek en fysische parameters zoals gemeten door WL in het Zeescheldebekken in 2015 (in Dutch). Versie 3.0. Tech. Rep. 12_070, Flanders Hydraulics Research, 167 pp.